Non-equilibrium fractionation during ice cloud formation in iCAM5: evaluating the common parameterization of supersaturation as a linear function of temperature

- Marina Dütsch¹, Peter N. Blossey¹, Eric J. Steig¹, and Jesse M. Nusbaumer²
- 1 University of Washington, Seattle, WA, United States of America $\,$
- ²National Center for Atmospheric Research, Boulder, CO, United States of America

Key Points:

13

- A linear function oversimplifies the dependence of supersaturation on temperature
 - The average relation between δD and deuterium excess is nevertheless reasonably well reproduced by a linear function
- With the model-predicted supersaturation, water isotopes can help constrain uncertain microphysical parameters

Corresponding author: Marina Dütsch, mduetsch@uw.edu

Abstract

15

16

17

18

19

20

21

22

23

25

26

27

28

29

30

31

32

35

36

37

38

39

40

42

43

44

45

46

Supersaturation with respect to ice determines the strength of non-equilibrium fractionation during vapor deposition onto ice or snow, and therefore influences the water isotopic composition of vapor and precipitation in cold environments. Historically, most general circulation models formed clouds through saturation adjustment and therefore prevented supersaturation. To match the observed isotopic content, especially the deuterium excess, of snow in polar regions, the saturation ratio with respect to ice (Si) was parameterized, usually by assuming a linear dependence of Si on temperature. The Community Atmosphere Model version 5 (CAM5) no longer applies saturation adjustment for the ice phase and thus allows ice supersaturation. Here, we adapt the isotope-enabled version of CAM5 to compute non-equilibrium fractionation in ice and mixed-phase clouds based on Si from the CAM5 microphysics, and use it to evaluate the common parameterization of Si. Our results show a wide range of Si predicted by the CAM5 microphysics and reflected in the simulated deuterium excess of Antarctic precipitation; this is overly simplified by the linear parameterization. Nevertheless, a linear function, when properly tuned, can reproduce the average observed relationship between δD and deuterium excess reasonably well. However, only the model-predicted Si can capture changes in microphysical conditions under different climate states that are not due to changes in temperature. Furthermore, parametric sensitivity tests show that with the model-predicted Si, water isotopes are more closely tied to the model microphysics and can therefore constrain uncertain microphysical parameters.

Plain language summary

The concentration of oxygen and hydrogen isotopes of water depends on meteorological processes such as evaporation from the ocean, and cloud formation. Water isotope concentrations measured in ice cores and other natural archives are therefore used to reconstruct Earth's past climate. In Antarctica, isotope concentrations strongly depend on the meteorological conditions during ice and mixed-phase cloud formation, especially the supersaturation with respect to ice. Isotope-enabled climate models, which are often used to support interpretations of isotope measurements, commonly prescribe supersaturation with respect to ice as a linear function of temperature. It is unknown how much this simplification affects the representation of water isotope concentrations in the models. Here we use a recently-developed isotope-enabled climate model, which

uses a physically-based calculation of supersaturation, to evaluate the linear parameterization used in other models. We find that, even though it is less physically realistic, the
linear parameterization can represent the average water isotope concentrations reasonably well. We also evaluate how model parameters related to supersaturation affect water isotopes. Our results suggest that water isotopes can potentially be used to improve
climate models.

1 Introduction

53

54

55

56

57

60

61

62

63

65

67

68

70

71

72

73

74

75

76

77

78

Stable water isotopologues (H₂¹⁶O, HD¹⁶O, H₂¹⁸O, hereafter referred to as stable water isotopes) have shown great potential as natural tracers of the global water cycle, and have provided valuable insight into Earth's past and present climate (e.g., Dansgaard et al., 1993; Markle et al., 2017; Moyer, Irion, Yung, & Gunson, 1996). The basis for their wide range of applications is isotopic fractionation, which occurs during phase transitions and is caused by the different thermodynamic properties of the isotopes: heavier water isotopes have higher binding energies and therefore preferentially go to the compound in which the molecules are bound most strongly. They also have slower diffusion velocities and therefore need more time to reach an equilibrium state. Due to these two effects, stable water isotopes experience equilibrium and non-equilibrium fractionation, respectively, and thereby continuously record the meteorological history of air parcels through changes in their relative concentrations. Equilibrium fractionation occurs during every phase transition involving the vapor phase and is roughly eight times stronger for HD¹⁶O than for H₂¹⁸O, leading to a ratio close to 8:1 between δ D and δ ¹⁸O in atmospheric waters, where the δ notation describes the concentration of HD¹⁶O and H₂¹⁸O relative to Vienna Standard Mean Ocean Water (VSMOW): $\delta = \frac{R}{R_{VSMOW}} - 1$; $R^{^{18}O} = \frac{R}{R_{VSMOW}} - 1$ $[^{18}O]/[^{16}O]; R^D = [D]/[H]$. Non-equilibrium fractionation occurs during phase transitions where diffusion is important, that is, (1) evaporation of water from the surface or from rain drops, when there is a strong gradient of humidity, and (2) ice and mixedphase cloud formation, which usually occurs in an environment that is supersaturated with respect to ice (Rogers, 1979). Non-equilibrium fractionation is stronger for H₂¹⁸O than for HD¹⁶O, and therefore leads to deviations from the ratio of 8:1, which are commonly quantified by the deuterium excess, $d = \delta D - 8 \cdot \delta^{18}O$ (Dansgaard, 1964). Due to the complexity of processes involving fractionation, measurements of sta-

ble water isotopes would be difficult to interpret without the help of numerical isotope

81

86

89

92

95

101

104

105

106

107

108

109

110

111

models. Since Dansgaard (1964) developed a Rayleigh model simulating isotopic vari-79 ations in an isolated air parcel to explain the temperature effect and the amount effect 80 (i.e., increasing depletion of heavy isotopes with decreasing temperature and increasing precipitation amount), numerical models have been widely applied to link measured iso-82 topic variations to physical processes. Following the pioneering work of Joussaume, Jouzel, 83 and Sadourny (1984) stable water isotopes have been incorporated into many atmospheric general circulation models (AGCMs): iCAM (Lee, Fung, DePaolo, & Henning, 2007; Nus-85 baumer, Wong, Bardeen, & Noone, 2017), ECHAMwiso (Hoffmann, Werner, & Heimann, 1998; Werner, Langebroek, Carlsen, Herold, & Lohmann, 2011), GISS ModelE (Schmidt, Hoffmann, Shindell, & Hu, 2005), HadCM3 (Tindall, Valdes, & Sime, 2009), ICON-ART-Iso (Eckstein et al., 2018), IsoGSM (Yoshimura, Kanamitsu, Noone, & Oki, 2008), and LMDZiso (Risi, Bony, Vimeux, & Jouzel, 2010) among others. These AGCMs solve the 90 full set of equations governing the dynamics and physics of the atmosphere on a global 91 three-dimensional grid, and simulate fractionation during all phase transitions in the hydrological cycle. In contrast to Rayleigh models, isotope-enabled AGCMs provide a spa-93 tially and temporally complete picture of global isotopic variations in water vapor and precipitation, limited only by their spatial resolution and the parameterization of unresolved processes. They have been widely applied to support interpretations of isotope measurements in paleoarchives. For example, Werner, Mikolajewicz, Heimann, and Hoffmann (2000) showed with the help of ECHAMwiso that seasonality of precipitation explains the discrepancy between borehole and isotope-derived temperatures in Greenland, and Sime, Wolff, Oliver, and Tindall (2009) showed with the help of HadCM3 that the 100 relation between temperature and isotope ratios in Antarctic ice cores is nonlinear and that therefore interglacial climates may have been warmer than previously thought. At 102 the same time, isotope tracers can be used to constrain physical parameterizations in the 103 models that could otherwise not be detected because of compensating errors in the moisture, pressure or temperature fields (Field et al., 2014; Nusbaumer et al., 2017; Risi et al., 2012). Historically, AGCMs use saturation adjustment to determine the rates of conden-

sation, evaporation, deposition, and sublimation to or from both liquid and ice phase condensate. Thus, supersaturation is removed after each time step by converting excess vapor to liquid or ice clouds. However, no supersaturation means no non-equilibrium fractionation during ice cloud formation, and thus unrealistic deuterium excess values, especially at high latitudes. To solve this problem, supersaturation with respect to ice in these models is parameterized and accounted for in the microphysical transfers of the heavy water isotopes (HD¹⁶O, H₂¹⁸O) but not in the microphysical treatment of standard water (H₂¹⁶O). In most AGCMs, the same parameterization as the one used in Rayleigh models is adopted, which describes the saturation ratio with respect to ice (Si) as a linear function of temperature (T) in the form of $Si = a + b \cdot T$ (Jouzel & Merlivat, 1984; Petit, White, Young, Jouzel, & Korotkevich, 1991). The intercept a is usually set to a value close to 1, implying saturation at $T \approx 0$ °C, while the slope b is adjusted such that the simulated deuterium excess matches observations, usually of snow in Antarctica (e.g., Petit et al., 1991). The resulting values for b range from b = -0.002 (Nusbaumer et al., 2017) to b = -0.007 (Schoenemann, Steig, Ding, Markle, & Schauer, 2014).

There are several limitations related to parameterizing supersaturation with respect to ice as a linear function of temperature: (1) a one-dimensional linear function cannot reflect a potential wide range of supersaturations at a given temperature, (2) since it is mostly tuned for present-day climate, the parameterization might not represent past climate conditions correctly, due to possible differences in the microphysics that influence supersaturation (e.g., different dust emissions or a different ratio of mixed-phase and ice clouds), and (3) since the isotope and microphysics parts of the model act independently in such a setup, an agreement between modeled and observed isotope ratios reflects on the quality of the tuning process rather than the quality of the model (Mathieu et al., 2002).

The Community Atmosphere Model version 5 (CAM5) (Neale et al., 2010) is one of a growing number of AGCMs whose microphysics scheme does not apply saturation adjustment for the ice phase and therefore allows supersaturation with respect to ice. This means that, although it is still used in the isotope-enabled version of CAM5 (iCAM5) (Nusbaumer et al., 2017), the parameterization of Si is not necessary. The aim of this study is therefore to adapt iCAM5 to compute non-equilibrium fractionation based on Si predicted by the microphysics scheme (Gettelman et al., 2010; Morrison & Gettelman, 2008), and with the help of this new model version (1) evaluate the parameterization of Si as a linear function of T, and (2) test the sensitivity of stable water isotopes to microphysical parameters influencing the model-predicted Si. Thereby we focus on Antarctica, where supersaturation during ice and mixed-phase cloud formation is especially important for isotopes in precipitation, and compare simulations in two different

climates, present day and the last glacial maximum. Both iCAM5 versions are validated against observations of isotopes in surface snow and ice cores from Antarctica.

2 Methods

2.1 Model

CAM5 (Neale et al., 2010) is the atmospheric component of the National Center for Atmospheric Research (NCAR) Community Earth System Model (CESM) (Hurrell et al., 2013). For stratiform cloud physics it uses the macrophysics scheme by Park, Bretherton, and Rasch (2014) and the two-moment microphysics scheme by Morrison and Gettelman (2008), modified to allow supersaturation with respect to ice by Gettelman et al. (2010). In pure ice clouds ($T < -37^{\circ}\mathrm{C}$), ice crystals can form via heterogeneous immersion freezing on mineral dust or by the homogeneous freezing of sulfate (Liu & Penner, 2005; Liu, Penner, Ghan, & Wang, 2007). Ice crystal formation in mixed-phase clouds ($-37^{\circ}\mathrm{C} < T < 0^{\circ}\mathrm{C}$) occurs via heterogeneous deposition nucleation and condensation freezing (Meyers, DeMott, & Cotton, 1992) and also through contact freezing (Young, 1974). Moist convection is separated into deep convection (Zhang & McFarlane, 1995) and shallow convection (Park & Bretherton, 2009), and moist boundary layer turbulence is parameterized following Bretherton and Park (2009).

The implementation of stable water isotopes in CESM (Brady et al., 2019) follows the approach of previous modeling work (e.g., Hoffmann et al., 1998; Joussaume et al., 1984; Yoshimura et al., 2008). $\mathrm{H}_2^{18}\mathrm{O}$ and $\mathrm{HD}^{16}\mathrm{O}$ were added and tracked throughout the model's hydrological cycle. Both heavy isotopes experience equilibrium and non-equilibrium fractionation during phase transitions. The equilibrium fractionation factors (α_{eq}), which describe the ratios of saturation vapor pressures of the heavy isotopes ($\mathrm{H}_2^{18}\mathrm{O}$, $\mathrm{HD}^{16}\mathrm{O}$) and the light isotope ($\mathrm{H}_2^{16}\mathrm{O}$), are parameterized as functions of T following Horita and Wesolowski (1994) for the liquid/vapor transition, and following Majoube (1971) and Merlivat and Nief (1967) for the ice/vapor transition. The ratios of diffusivities of the light and heavy isotopes (D/D_{iso}), which are important for non-equilibrium fractionation, are taken from Merlivat (1978). In iCAM5 (Nusbaumer et al., 2017), fractionation during evaporation from the ocean is parameterized with the Craig and Gordon (1965) model using a wind speed dependent formulation of the non-equilibrium fractionation factor (Merlivat & Jouzel, 1979). A similar approach is used for evapotranspiration from land in the isotope-enabled Community Land Model version 4 (iCLM4) (Wong, Nusbaumer,

& Noone, 2017) that is coupled to iCAM5. Sublimation of surface snow or ice is assumed to occur without fractionation. The snow depth in iCLM4 is limited to a maximum snow water equivalent of $H_{max} = 1$ m, and any precipitation that would increase the snow depth to $H > H_{max}$ is routed directly to runoff (i.e., to the river component and ultimately to the ocean). This means that the isotopic composition of the snow pack is not updated in such regions. In the following, the implementation of fractionation during ice cloud formation, which is the focus of this study, is described in more detail. For a detailed description of other isotope parameterizations in iCAM5, see Nusbaumer et al. (2017).

2.1.1 Fractionation during ice cloud formation

Because of the low diffusivities of water molecules in ice and the short lifetime of ice crystals in the atmosphere, vapor deposition onto ice or snow is assumed to follow a Rayleigh process, which describes isotopic fractionation in an open system, where the condensate is immediately removed. The isotope ratio of the condensate (R_c) and the remaining vapor (R_v) are then given by:

$$R_c = \alpha \cdot R_{v,0} \tag{1}$$

$$R_v = R_{v,0} \cdot f^{\alpha - 1} \tag{2}$$

where $R_{v,0}$ is the initial isotope ratio in the vapor, f is the fraction of remaining vapor, and α is the effective fractionation factor (including both equilibrium and non-equilibrium fractionation). α is calculated following Jouzel and Merlivat (1984) and Blossey, Kuang, and Romps (2010):

$$\alpha = \frac{\alpha_{eq} \cdot Si}{\alpha_{eq} \cdot \frac{D}{D_{ieo}} \cdot (Si - 1) + 1}$$
(3)

where D and D_{iso} are the diffusivities of the light and the heavy isotopes, respectively, Si is the saturation ratio with respect to ice, and α_{eq} is the equilibrium fractionation factor. In the default iCAM5 setup, Si is parameterized as a linear function of T, as in most previous modeling studies (e.g., Jouzel & Merlivat, 1984; Petit et al., 1991; Risi et al., 2010; Werner et al., 2011):

$$Si = a + b \cdot T \tag{4}$$

with the tuning parameters a and b set to 1.0 and -0.002, respectively, in order to match observed precipitation deuterium excess over Antarctica (Nusbaumer et al., 2017).

To illustrate the impact of this parameterization, Figure 1 shows the evolution of δD and deuterium excess in vapor and condensate described by the Rayleigh equations (Equations 1 and 2 above) for three hypothetical air parcels with an initial vapor isotopic composition of $\delta D = -160\%$ and $\delta^{18}O = -20\%$, and different parameterizations of Si as a linear function of T. The air parcels are assumed to cool from $T = -10^{\circ} C$ to $T = -50^{\circ} C$ with $\sim 10\%$ of vapor condensing (to ice only) per $1^{\circ} C$ of cooling, such that the fraction of remaining vapor f = 2% at $T = -50^{\circ} C$.

We evaluate the effects of non-equilibrium fractionation in the δD vs. deuterium excess phase space, because it has been widely used in the past to analyze the effect of Si on isotopes (e.g., Petit et al., 1991; Risi et al., 2010; Werner et al., 2011). Since heavy isotopes condense more readily than light isotopes, the condensate has a higher δD than the vapor it originates from in all three air parcels. As more vapor condenses, the removal of heavy isotopes leads to lower δD in both vapor and newly forming condensate. The deuterium excess in vapor and condensate decreases first and then increases again. This curvature is due to an artifact of the traditional deuterium excess definition related to the nonlinearity of the δ -scale (where the change of δ depends on δ itself), and could be avoided by using a definition based on the $\ln(R)$ scale (Dütsch, Pfahl, & Sodemann, 2017; Markle et al., 2017). However, here we focus on the differences between the lines and therefore the curvature is of advantage, because it makes the differences more visible.

Initially, at high δD , a higher Si leads to a higher deuterium excess in the condensate and a lower deuterium excess in the remaining vapor, due to stronger non-equilibrium fractionation (i.e., $HD^{16}O$ diffuses more readily onto the ice crystals than $H_2^{18}O$ due to its larger diffusivity). However, because of the lower deuterium excess in the remaining vapor, the newly forming condensate has a lower deuterium excess as well, and after further deposition the Rayleigh lines of the condensate cross. For small fractions of remaining vapor, a higher Si therefore leads to a lower deuterium excess in the condensate. Such small fractions of remaining vapor are typically found at high latitudes or altitudes. Furthermore, a higher Si leads to an overall flatter slope between δD and deuterium excess. Thus, Figure 1 demonstrates that Si has a large impact on the deuterium excess in both vapor and condensate, and therefore a correct representation of Si in isotope models is important.

In contrast to most AGCMs, the microphysics scheme of CAM5 allows Si > 100% (Gettelman et al., 2010), and the parameterization of Si is no longer necessary. Now va-

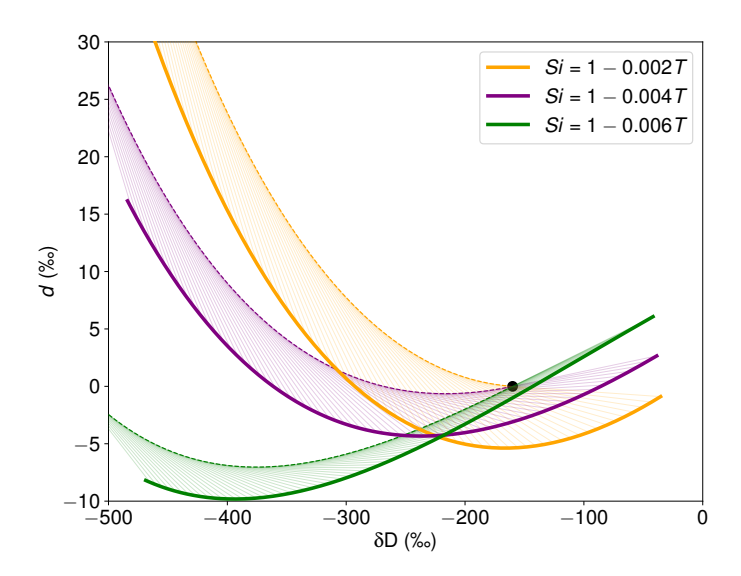


Figure 1. Evolution of δD and deuterium excess in water vapor (dashed lines) and condensate (solid lines) during Rayleigh condensation for three different parameterizations of Si as a function of T. The black dot depicts the initial isotopic composition of the water vapor and the thin lines connect the isotopic composition of the condensate with the isotopic composition of the vapor it originates from.

por deposition onto ice and snow can be treated consistently for standard water ($H_2^{16}O$) and the heavy isotopes ($HD^{16}O$ and $H_2^{18}O$). In this study, we therefore adapt the computation of non-equilibrium fractionation in iCAM5 to use Si predicted by the microphysics scheme (hereafter referred to as Si_{real}) instead of the parameterized Si (hereafter referred to as Si_{param}).

Note that the default iCAM5 setup limits non-equilibrium fractionation during ice and mixed-phase cloud formation to $T < -20^{\circ}$ C, whereas in reality it can occur at $T < 0^{\circ}$ C if Si > 100%. For consistency this -20° C limit is kept in the modified iCAM5 version, but will be the focus of sensitivity tests (see Section 2.2.2).

2.2 Simulations

2.2.1 Control simulations

We run four control (ctrl) iCAM5 simulations, one for each of the Si versions (Si_{param} and Si_{real}) used in two different climates (present day and last glacial maximum). All four simulations use the finite-volume dynamical core with 1.9°N×2.5°E horizontal res-

olution and a hybrid sigma-pressure vertical coordinate system with 30 levels. iCAM5 is coupled to the isotope-enabled land surface model iCLM4 (Wong et al., 2017) and the isotope-enabled sea ice model iCICE4 (Brady et al., 2019), with prescribed sea surface temperatures and sea ice concentrations. Present-day climate simulations use year 2000 CE climate forcings, and sea surface temperatures and sea ice concentrations from Hurrell, Hack, Shea, Caron, and Rosinski (2008). Last glacial maximum simulations use year 19050 BCE (21000 BP(1950)) climate forcings, and sea surface temperatures and sea ice concentrations from Zhu et al. (2017). Aerosol emissions are based off historical data from Lamarque et al. (2010) and Lamarque et al. (2011). Ocean isotope ratios are assumed to be constant in time and space ($\delta^{18}O = 0\%$ and $\delta D = 0\%$ in present-day climate, and $\delta^{18}O = 1.13\%$ and $\delta D = 9.10\%$ during the last glacial maximum, which corresponds to the climatological global average from Zhu et al. (2017)). For both climates, the simulations are branched from a one-year spin-up simulation using Si_{param} and run for ten years (Table 1). In addition to the Si_{param} simulations where the tuning parameter b in Equation 4 is set to the default value (b = -0.002), we run two simulations for present-day climate and last glacial maximum with b = -0.004 and b = -0.006, respectively. The results of these simulations will be shown in Figure 6 and in the supporting information.

2.2.2 Sensitivity tests

255

256

257

258

259

260

261

262

265

266

267

268

269

270

271

272

275

276

277

278

279

280

281

282

285

286

Since stable water isotopes are sensitive to Si, and Si is predicted by the microphysics scheme in the Si_{real} simulations, isotopes can potentially be used to constrain microphysical parameters influencing Si in the model. This is especially useful because measurements of Si itself are sparse (Genthon et al., 2017). We select three microphysical parameters that significantly influence Si: the number of active aerosols for ice nucleation (naai), the Wegener-Bergeron-Findeisen time scale for the growth of ice crystals (epsi), and the sedimentation velocity of ice crystals (ai). To test the sensitivity of stable water isotopes to these parameters we run additional simulations for present-day climate, in which we scale the parameters by a factor β , where $\beta = 0.5, 2$.

Furthermore, we test the sensitivity of stable water isotopes to the temperature threshold (T_{ini}) below which non-equilibrium fractionation occurs for both Si versions, also in present-day climate. In addition to the control simulations using $T_{ini} = -20^{\circ}$ C, we run simulations with $T_{ini} = -10^{\circ}$ C and $T_{ini} = 0^{\circ}$ C. All sensitivity simulations are

Table 1. Overview of simulations. Control simulations are run for present-day climate (PD) and the last glacial maximum (LGM). Sensitivity simulations are run for present-day climate only. T_{ini} is the temperature threshold for non-equilibrium fractionation, naai is the number of active aerosols for ice nucleation, epsi is the Wegener-Bergeron-Findeisen time scale for the growth of ice crystals, and ai is the sedimentation velocity of ice crystals.

control simulations (10 years)	sensitivity simulations (5 years)
LGM, Si_{param} , $b = -0.002$	PD, Si_{param} , $naai~(\times 0.5, \times 2)$
LGM, Si_{param} , $b = -0.004$	PD, Si_{param} , $epsi$ (×0.5,×2)
LGM, Si_{param} , $b = -0.006$	PD, Si_{param} , $ai~(\times 0.5, \times 2)$
LGM, Si_{real}	PD, Si_{param} , T_{ini} (= -10°C, = 0°C)
PD, Si_{param} , $b = -0.002$	PD, Si_{real} , $naai~(\times 0.5, \times 2)$
PD, Si_{param} , $b = -0.004$	PD, Si_{real} , $epsi$ (×0.5, ×2)
PD, Si_{param} , $b = -0.006$	PD, Si_{real} , $ai~(\times 0.5, \times 2)$
PD, Si_{real}	PD, Si_{real} , T_{ini} (= -10°C, = 0°C)

branched from the present-day one-year spin-up simulation using Si_{param} (and $\beta=1$, $T_{ini}=-20^{\circ}$) and run for five years (Table 1).

2.3 T, Si, and deuterium excess in vapor during cloud formation

Over Antarctica, most precipitation falls in the form of snow, which, in contrast to rain, does not experience strong fractionation during sublimation and thus carries its initial isotopic signal all the way to the ground. The deuterium excess in surface snow therefore strongly depends on the meteorological conditions (T and Si), as well as the isotopic composition of the vapor (δD_v and $\delta^{18}O_v$) at cloud formation. To determine these variables we add four new diagnostic water tracers to iCAM5, whose deposition and condensation fluxes to ice and liquid clouds in the microphysics scheme are equal to the fluxes of standard water multiplied by T, Si, δD_v and $\delta^{18}O_v$, respectively (Figure 2, red arrows). The ratio of tracer cloud mixing ratio to standard water cloud mixing ratio is thus equal to the value the variables had at the locations and times the cloud formed, weighted by the fluxes of standard water. By preserving this tracer ratio for fluxes between clouds and precipitation (Figure 2, blue arrows) these values can be traced all the way to where precipitation falls. To ensure the tracer ratio corresponds to the conditions at cloud formation, the vapor phase of the tracers has to be equal to standard water vapor. This

is done by setting tracer fluxes to and from vapor equal to the fluxes of standard water (Figure 2, black arrows). Note that with this method fluxes away from the source can differ from the fluxes to the destination (cf. Figure 2a and 2b), which violates mass conservation. For example, in the case of rain evaporation, the flux away from the source (rain) is equal to the flux of standard water multiplied by the tracer ratio in rain, while the flux to the destination (vapor) is equal to the flux of standard water. This is not a problem, because these tracers are purely diagnostic.

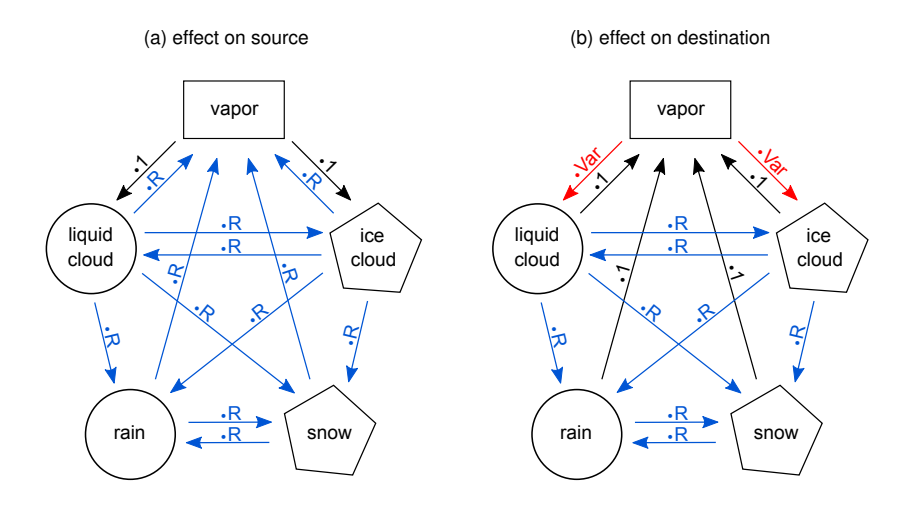


Figure 2. Microphysical processes in iCAM5. The shapes show the five physical states of water allowed in the microphysics scheme. The arrows show transitions between the five states and are colored by the type of multiplication applied for the T, Si, δD_v and $\delta^{18}O_v$ tracers for (a) the source of the flux and (b) the destination of the flux. Red: the flux of standard water multiplied by T, Si, δD_v or $\delta^{18}O_v$; blue: the flux of standard water multiplied by the tracer ratio; black: the flux of standard water. For example, in the case of rain evaporation, rain is the source and vapor is the destination, or in the case of snow melting, snow is the source and rain is the destination.

2.4 Observations

The simulated isotope ratios are compared with ice core measurements from five Antarctic sites: West Antarctic Ice Sheet (WAIS) Divide (WD) (Markle et al., 2017; WAIS Divide Project Members, 2013, 2015), European Project for Ice Coring in Antarctica (EPICA) Dronning Maud Land (EDML) (EPICA Community Members, 2006; Stenni et al., 2010), EPICA Dome C (EDC) (Jouzel et al., 2007; Stenni et al., 2010), Talos Dome (TAL) (Buiron et al., 2012; Landais et al., 2015; Stenni et al., 2011), and South Pole (SP) (Kahle,

Holme, Jones, Gkinis, & Steig, 2018), all placed on a common time scale by Buizert et al. (2018). The ice core data are averaged from 1000 BCE to 2000 CE for present-day climate and from 19000 to 16000 BCE (20950 to 17950 BP(1950)) for the last glacial maxmimum. The present-day simulations are additionally compared with measurements of Antarctic surface snow from Masson-Delmotte et al. (2008).

3 Results

3.1 Spatial pattern of deuterium excess

Figure 3 shows the climatology of deuterium excess in precipitation for the four control simulations, and their differences (see supporting information Figures S1 and S2 for the Si_{param} simulations with b=-0.004 and b=-0.006, respectively). In all four simulations, deuterium excess decreases with latitude over the ocean, reaching values close to 0% around 70° S (Figure 3 a,b,d,e). The decrease can partly be explained by an increasing fraction of snow in precipitation. Over Antarctica, deuterium excess is negative at the coast and positive further inland, reaching values of up to 20% close to the south pole. Higher deuterium excess values inland can also be seen in the ice cores, and are related in part to the nonlinear effect of the δ scale (Dütsch et al., 2017; Markle et al., 2017).

In iCAM5, the deuterium excess during the last glacial maximum is generally lower over the ocean and higher over central Antarctica than in present-day climate (Figure 3 c,f). The deuterium excess predicted by the different Si versions differs substantially over Antarctica (Figure 3 g,h) and over Greenland (not shown), indicating the presence of non-equilibrium fractionation during ice and mixed-phase cloud formation and therefore the sensitivity of precipitation isotopes to Si in very cold regions. The model-predicted saturation ratio with respect to ice, Si_{real} , leads to lower deuterium excess than Si_{param} with b = -0.002, similar deuterium excess as Si_{param} with b = -0.004 and higher deuterium excess than Si_{param} with b = -0.006. The differences are most pronounced during the last glacial maximum. At the coast of Antarctica, the Si versions even show opposite trends between last glacial maximum and present day climate. Si_{real} produces lower deuterium excess values during the last glacial maximum than in present-day climate, while Si_{param} produces higher or lower values, depending on the choice of b. The ice cores close to the coast of Antarctica also have lower deuterium excess values during the last glacial maximum than in present-day climate, in agreement with the Si_{real} simulations. δD and

 δ^{18} O alone do not differ much between the Si_{param} and Si_{real} simulations relative to their spatial and temporal variations (see supporting information Figures S3 and S4). This is because they are primarily governed by equilibrium fractionation.

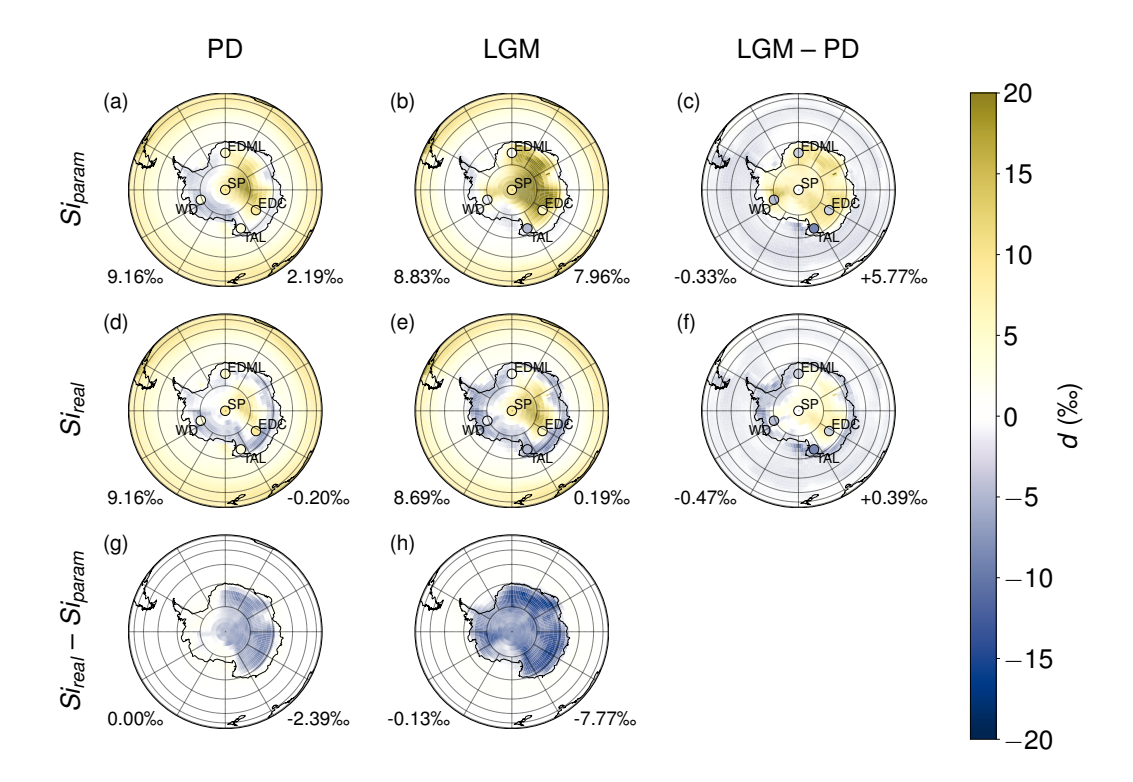


Figure 3. Climatology of deuterium excess in precipitation. Top: Si_{param} simulations (with b = -0.002), center: Si_{real} simulations, bottom: difference between the Si_{real} and Si_{param} simulations. Left: present day (PD), center: last glacial maximum (LGM), right: difference between last glacial maximum and present day. Numbers to the left and right of the Earth denote the global and Antarctic averages, respectively. The ice core measurements are shown as dots.

3.2 Relationship between T and Si

Figure 4 shows at which T and Si most Antarctic precipitation forms in iCAM5 (using the diagnostic water tracers described in Section 2.3). 90% of Antarctic precipitation forms at T between -42° C and -14° C in present-day climate (Figure 4a) and between -50° C and -20° C during the last glacial maximum (Figure 4b). Si is mostly between 107% and 127% in present-day climate and between 107% and 130% during the last glacial maximum. Thus, despite much lower T, precipitation during the last glacial maximum does not form at significantly higher Si. The differences in occurrence frequency

between the last glacial maximum and present-day climate also show a much more complex pattern than a simple shift to lower T and higher Si (Figure 4c).

In both climates, Si is close to 100% at $T \approx 0$ °C, and increases with decreasing T as the ratio between the saturation vapor pressure over liquid water and ice increases. However, the increase of Si with decreasing T is not linear. The mean Si increases non-linearly with decreasing T and is always higher than the default Si_{param} with b = -0.002. Furthermore, for every depicted T there is a wide range of possible Si values, sometimes spanning more than 50%.

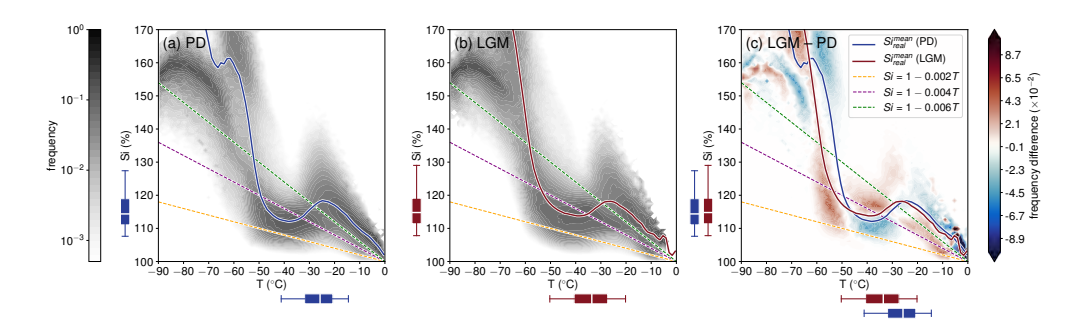


Figure 4. Precipitation-weighted occurrence frequency of T and Si at cloud formation calculated from 6-hourly average precipitation fields over Antarctica for (a) present day (PD), (b) last glacial maximum (LGM), (c) the difference between last glacial maximum and present day. The frequencies are calculated separately for each T bin of 1.2° C. The solid lines are the precipitation-weighted mean Si_{real} for PD and LGM, and the dashed lines show $Si_{param} = 1 - 0.002 \cdot T$, $Si_{param} = 1 - 0.004 \cdot T$, and $Si_{param} = 1 - 0.006 \cdot T$. The boxplots indicate at which T and Si most precipitation forms (horizontal: T, vertical: Si, blue: PD, red: LGM) with the whiskers showing the 5th and 95th percentile.

As Figure 5 shows, the differences between Si_{real} and Si_{param} also affect the deuterium excess. If $Si_{real} < Si_{param}$, the resulting deuterium excess in precipitation in the Si_{real} simulations is always lower than in the Si_{param} simulations with b = -0.002 (Figure 5a,d). If $Si_{real} > Si_{param}$, the signal is mixed: at relatively high T (> -37° C), the resulting deuterium excess in precipitation is higher in the Si_{real} simulations than in the Si_{param} simulations with b = -0.002; at relatively low T (< -37° C), it is generally lower in the Si_{real} simulations than in the Si_{param} simulations with b = -0.002. This pattern is the result of two additive effects: the difference in the strength of non-equilibrium fractionation, and the difference in the isotopic composition of the vapor from

which clouds form. Non-equilibrium fractionation is stronger for higher Si and therefore the difference between deuterium excess in precipitation (d_p) and deuterium excess in vapor (d_v) is larger in the Si_{real} simulations than in the Si_{param} simulations where $Si_{real} > Si_{param}$, and smaller where $Si_{real} < Si_{param}$ (Figure 5b,e). Because Si_{real} is usually higher than Si_{param} with b = -0.002, the stronger non-equilibrium fractionation removes more deuterium excess from the remaining vapor, and therefore the deuterium excess in the remaining vapor is always lower in the Si_{real} simulations than in the Si_{param} simulations with b = -0.002 (Figure 5c,f). The opposite happens for Si_{param} with b = -0.004 and b = -0.006 (see supporting information Figures S5 and S6), because in these cases Si_{real} is usually lower than Si_{param} . The effect of fractionation dominates at relatively high $T (> -37^{\circ}C)$, leading to higher deuterium excess in the Si_{real} simulations where $Si_{real} > Si_{param}$ and vice versa, while the effect of the vapor dominates at relatively low $T (< -37^{\circ})$, leading to lower deuterium excess in the Si_{real} simulations compared to Si_{param} with b = -0.002 for all Si (and higher deuterium excess compared to Si_{param} with b = -0.004 and b = -0.006).

3.3 Relationship between δD and deuterium excess

Figure 6 shows the relationship between δD and deuterium excess in precipitation in the control simulations and observations. In addition to the Si_{param} simulation with the default b=-0.002, the simulations with b=-0.004 and b=-0.006 are shown in panels c and d. Note the similarity between the polynomial fits and the Rayleigh lines in Figure 1 including the crossing points, indicating that the isotopic composition of precipitation over Antarctica can be approximated by a Rayleigh process.

The simulated δD and deuterium excess values interpolated to the ice core sites tend to be more enriched along the polynomial fits compared to the observations. This may be related to the relatively coarse resolution and consequently lower topography. The advantage of the δD vs. deuterium excess phase space is that we can still infer what the deuterium excess would be at the ice core sites if δD was lower.

The simulations using Si_{real} and Si_{param} with b = -0.002 and b = -0.004, respectively, all produce a reasonable relation between δD and deuterium excess in present-day climate (Figure 6a,c). In contrast, the simulation using Si_{param} with b = -0.006 differs substantially from the observations, with too low deuterium excess values at lower δD (< -300%). All simulations underestimate deuterium excess at higher δD (> -300%),

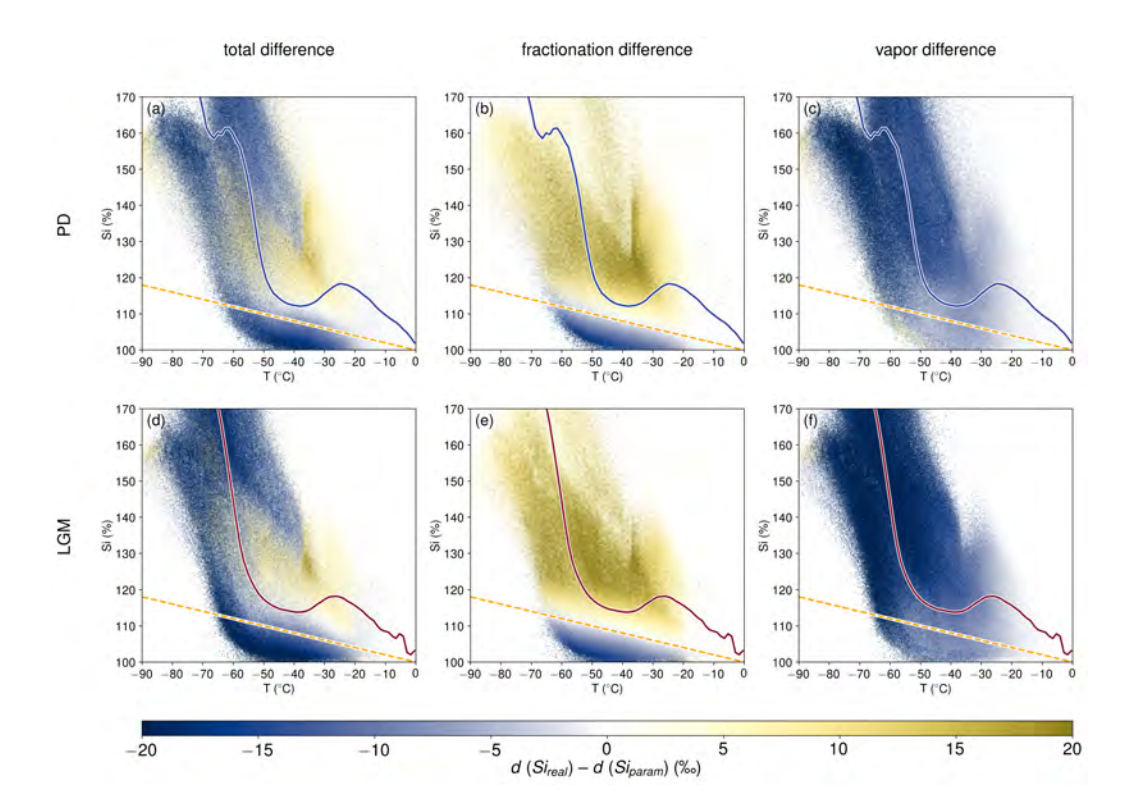


Figure 5. Difference in precipitation deuterium excess between the Si_{real} simulations and Si_{param} simulations with b = -0.002 as a function of T and Si at cloud formation for (a–c) present day (PD) and (d–f) last glacial maximum (LGM): (a,d) total difference in precipitation deuterium excess (d_p) , (b,e) difference resulting from fractionation during cloud formation $(d_p - d_v)$, (c,f) difference resulting from deuterium excess in vapor (d_v) . Each dot is a 6-hourly average at a grid point over Antarctica. The sum of (b) and (c) is equal to (a) and the sum of (e) and (f) is equal to (d). The dashed and solid lines are $Si_{param} = 1 - 0.002 \cdot T$ and the precipitation-weighted mean Si_{real} , respectively.

which might be related to evaporation from the ocean or land and is not further addressed in this study. The Si_{param} simulation with b = -0.002 produces lower deuterium excess values at higher δD and higher deuterium excess at lower δD compared to the Si_{real} simulation, which can be explained by the fact that the default parameterization mostly underestimates Si in iCAM5 as seen in Figure 4, leading to weaker non-equilibrium fractionation and a higher deuterium excess in the remaining water vapor (cf. Figure 1).

For the last glacial maximum there are only five observational data points, but they clearly fall within the range of values in the simulation using Si_{real} (except for EDC), while they are overestimated by the simulation using Si_{param} with b = -0.002 (Fig-

ure 6b,d). The simulation using Si_{param} with b=-0.004 produces more reasonable δD and deuterium excess values, but none of the Si_{param} simulations capture the range of the ice core values as well as the Si_{real} simulation does.

Thus, even though Figure 4 showed that Si is not a linear function of T, Si_{param} can represent the 10-year average relationship between δD and deuterium excess reasonably well. However, there is no guarantee that this is true in all situations. The large variability of Si at a given temperature might be important at shorter time scales, e.g.,

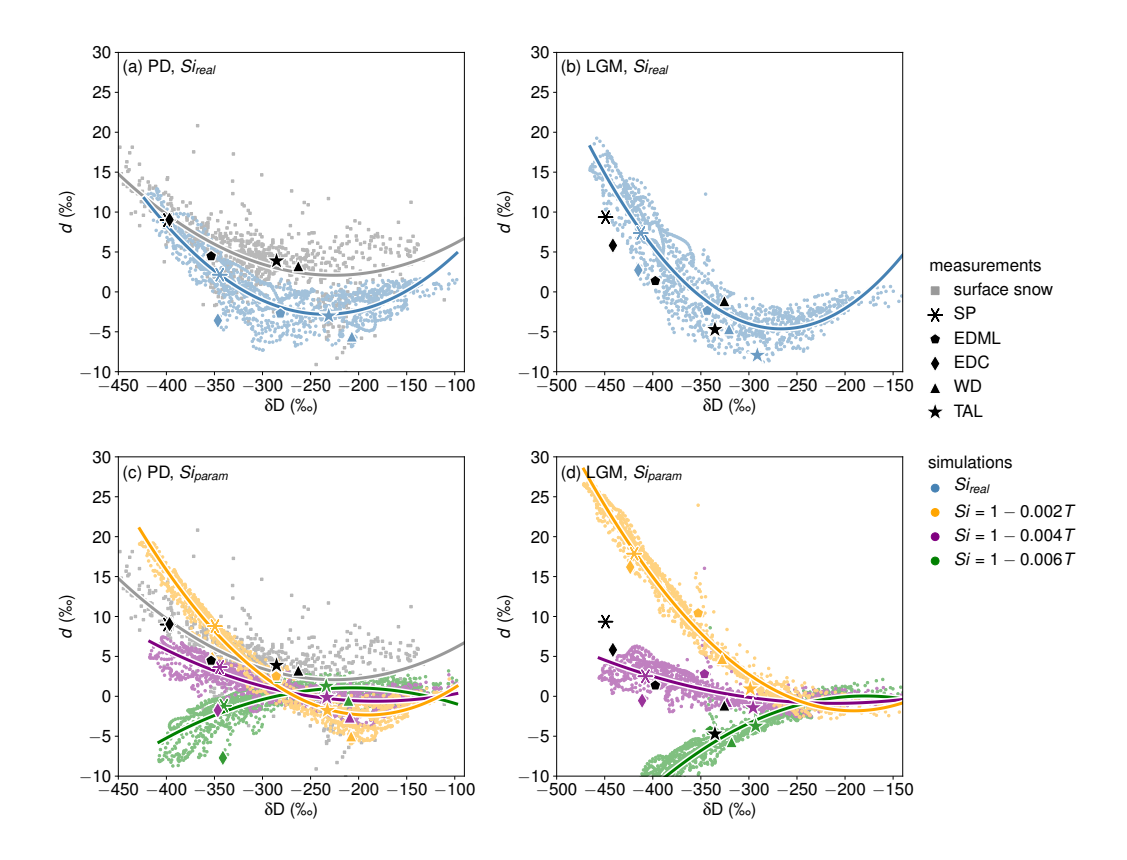


Figure 6. Simulated climatological δD and deuterium excess in precipitation at each grid point over Antarctica and the five ice cores sites (linearly interpolated from the four surrounding grid points) compared to observations for (a,c) present day (PD) and (b,d) last glacial maximum (LGM). The top row (a,b) shows the simulations using Si_{real} , the bottom row (c,d) shows the simulations using Si_{param} with b = -0.002 (orange), b = -0.004 (purple), and b = -0.006 (green), respectively. The grey dots are the measurements from Masson-Delmotte et al. (2008), and the black markers are the ice core measurements. The solid lines are quadratic polynomial fits of the dots.

for individual weather events, or in different regions, e.g. in the upper troposphere. Therefore, we recommend using the more physically realistic Si_{real} when possible.

3.4 Sensitivity tests

426

427

428

429

430

431

432

433

434

435

436

438

439

440

441

442

443

444

445

449

450

451

452

453

454

455

456

3.4.1 Microphysical parameters

This section addresses the sensitivity of the deuterium excess in Antarctic precipitation to the number of active aerosols for ice nucleation (naai), the Wegener-Bergeron-Findeisen time scale for the growth of ice crystals (epsi), and the sedimentation velocity of ice crystals (ai). By changing the properties of ice and mixed-phase clouds, these parameters directly influence Si. Furthemore, through feedbacks of clouds on climate, they indirectly influence T as well. In the Si_{param} simulations, the deuterium excess is sensitive only to T, because Si is parameterized as a linear function of T. In the Si_{real} simulations, the deuterium excess is sensitive to both T and Si. Figure 7 shows how Tand Si are affected by the scaling of the microphysical parameters in present-day climate. Higher naai and epsi increase ice nucleation and deposition, respectively, and thus reduce supersaturation, leading to lower Si at all temperatures (Figure 7a,b). Higher aienhances the sedimentation of ice crystals, with a mixed effect on Si. Higher values of ai result in lower Si above -30° C and higher Si below -30° C (Figure 7c). On average, scaling all three microphysical parameters by $\beta = 2$ compared to $\beta = 0.5$ leads to higher T and lower Si. According to the Rayleigh lines in Figure 1, we therefore expect lower deuterium excess at high δD and higher deuterium excess at low δD in Antarctic precipitation for $\beta = 2$ than for $\beta = 1$ in both the Si_{param} and the Si_{real} simulations, and the opposite effect for $\beta = 0.5$.

As Figure 8 shows, the lower Si and higher T in the simulations with $\beta=2$ indeed lead to a lower deuterium excess at high δD and a higher deuterium excess at low δD compared to the control simulation (vice versa for $\beta=0.5$). For all three parameters, the relation between δD and deuterium excess is similar across the Si_{param} simulations, because the effect of changes in β on T alone is relatively small. In contrast, the deuterium excess in the Si_{real} simulations is very sensitive to changes in Si caused by changes in β . Since the initial isotopic composition of the vapor depends on processes that are not addressed in this study (e.g., evaporation from the ocean or land) we will not focus on the absolute values, but on the slope between δD and deuterium excess in-

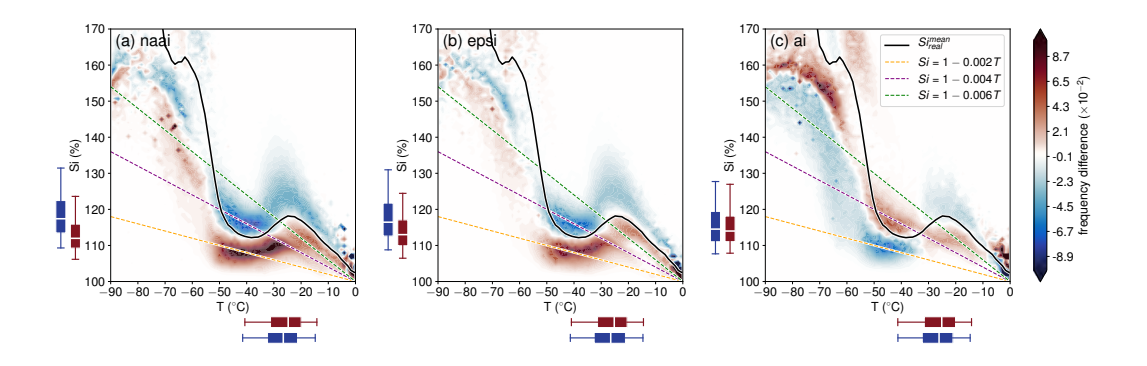


Figure 7. Difference in precipitation-weighted occurrence frequency of T and Si at cloud formation between the simulations with $\beta=2$ and $\beta=0.5$ calculated from 6-hourly average precipitation fields over Antarctica for (a) naai, (b) epsi, (c) ai. The solid line is the precipitation-weighted mean Si_{real} , and the dashed lines show $Si_{param}=1-0.002 \cdot T$, $Si_{param}=1-0.004 \cdot T$, and $Si_{param}=1-0.006 \cdot T$. The boxplots indicate at which T and Si most precipitation forms (horizontal: T, vertical: Si, blue: $\beta=0.5$, red: $\beta=2$) with the whiskers showing the 5th and 95th percentile.

stead. While the slope between deuterium excess and δD is too steep compared to observations in the Si_{real} control simulation, it is too flat in the Si_{real} simulations with reduced naai and epsi, suggesting that the truth lies somewhere in between. Reducing ai leads to lower deuterium excess at low δD , but with a similar slope between deuterium excess and δD .

3.4.2 Temperature threshold for non-equilibrium fractionation

Figure 9 shows how δD and deuterium excess depend on the temperature threshold below which non-equilibrium fractionation occurs during ice and mixed-phase cloud formation (T_{ini}) . Increasing T_{ini} from -20° C to -10° C or 0° C results in much lower deuterium excess values in the Si_{real} simulations (Figure 9b), whereas the values in the Si_{param} simulations do not depend strongly on T_{ini} (Figure 9a). This can be explained by the difference between Si_{real} and Si_{param} at relatively high T (> -20°) (cf. Figure 4a). While Si_{param} (with b = -0.002) only grows as large as 104% for $T > -20^{\circ}$ C, Si_{real} exceeds 110% in most instances when -20° C < $T < -10^{\circ}$ C. Therefore, Si_{real} leads to stronger non-equilibrium fractionation than Si_{param} , which leaves the remaining vapor (and consequently the newly forming condensate) depleted in deuterium excess. Interestingly, the effect of increasing T_{ini} is highly nonlinear. The difference between the simulations with

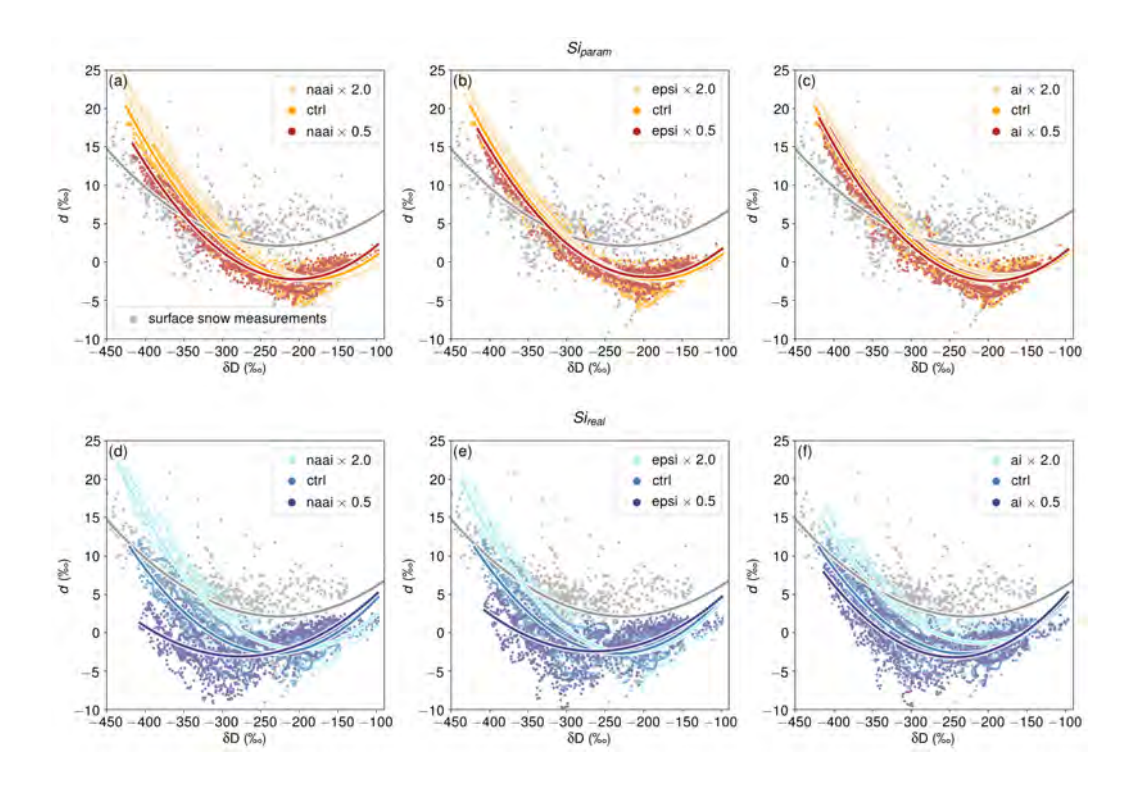


Figure 8. δ D and deuterium excess in precipitation in the sensitivity simulations for (a,d) naai, (b,e) epsi, (c,f) ai compared to observations (in present-day climate). The top row (a-c) shows Si_{param} with b=-0.002 and the bottom row (d-f) shows Si_{real} . The colored dots are the climatological averages at each grid point over Antarctica (dark: $\beta=0.5$, medium: $\beta=1$ (ctrl), light: $\beta=2$), and the grey dots are the observations from Masson-Delmotte et al. (2008). The solid lines are quadratic polynomial fits of the dots.

 $T_{ini} = -20^{\circ}\text{C}$ and $T_{ini} = -10^{\circ}\text{C}$ is much larger than the difference between the simulations with $T_{ini} = -10^{\circ}\text{C}$ and $T_{ini} = 0^{\circ}\text{C}$, suggesting that deposition onto ice and snow at T between -20°C and -10°C dominates the changes in both simulations with increased T_{ini} .

4 Discussion

476

477

478

479

480

481

482

483

4.1 Implications

Even though our results show that Si is clearly not a linear function of temperature, the Si_{param} simulations, with the right tuning, produced a reasonable range of δD and deuterium excess in Antarctic precipitation, both compared to observations and to Si_{real} simulations. In part this is not surprising, because the Si function had been tuned

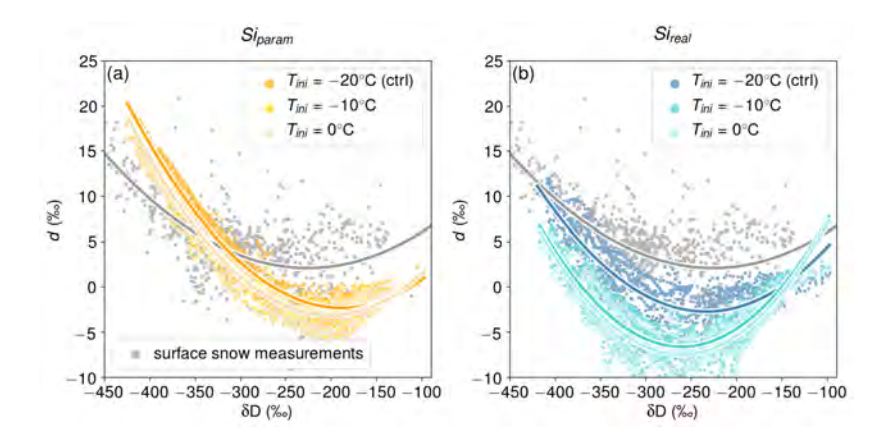


Figure 9. δD and deuterium excess in precipitation in the sensitivity simulations for different T_{ini} (the temperature threshold below which non-equilibrium fractionation occurs) compared to observations (in present-day climate). The left hand side (a) shows Si_{param} with b=-0.002 and the right hand side (b) shows Si_{real} . The colored dots are the climatological averages at each grid point over Antarctica (dark: $T_{ini}=-20^{\circ} C$ (ctrl), medium: $T_{ini}=-10^{\circ} C$, light: $T_{ini}=0^{\circ} C$), and the grey dots are the observations from Masson-Delmotte et al. (2008). The solid lines are quadratic polynomial fits of the dots.

for the simulations to match the observations. Nevertheless, this means that models parameterizing Si as a linear function of T are still a valid tool for supporting the interpretation of isotope measurements in paleoarchives. However, there may be situations where the large Si variability independent of T is important, e.g., for individual weather events. This variability can be represented only if Si is predicted by the microphysics scheme.

Furthermore, with Si predicted by the microphysics scheme, isotopes can serve as an additional observational constraint on microphysical parameters. Previous studies have shown that CAM5 tends to produce too much ice and too little supercooled liquid water in mixed-phase clouds (Cesana, Waliser, Jiang, & Li, 2015; Kay et al., 2016; Komurcu et al., 2014; Wall, Hartmann, & Ma, 2017). This means that even if Si is simulated perfectly, the overestimated ice production can lead to too many non-equilibrium fractionation events and a lower deuterium excess in the remaining vapor, which is passed to precipitation forming further downstream. The ice bias in CAM5 can be caused by a too efficient Wegener-Bergeron-Findeisen process, i.e., a too rapid growth of ice crystals at the expense of supercooled liquid water (Tan, Storelymo, & Zelinka, 2016), and is often

corrected for by decreasing the parameter epsi (e.g., Sagoo & Storelymo, 2017; Tan & Storelymo, 2016). Our simulation with reduced epsi has a flatter slope between δD and deuterium excess, suggesting that epsi might indeed be too high in the default CAM5 setup. Other studies have shown that CAM5's ice nucleation scheme for mixed-phase clouds (Meyers et al., 1992) overestimates the concentration of ice nucleating particles at high latitudes (DeMott et al., 2010; Prenni et al., 2007; Xie, Liu, Zhao, & Zhang, 2013), which also leads to too much ice in mixed-phase clouds. This is because the Meyers et al. (1992) scheme calculates ice nucleating particle concentration assuming a fixed dependence on T and Si based on measurements from the Sierra Nevada, where ice nucleating particles are much more abundant than at high latitudes, and does not take into account the spatial and temporal variability of ice nucleating particles. With most of Antarctic precipitation in our simulations forming in the mixed-phase cloud regime (-37° C < T < 0°C), naai is primarily predicted by the Meyers et al. (1992) scheme, and our results show that reducing naai improves the slope between δD and deuterium excess as well. The overestimated ice fraction in mixed-phase clouds may also explain why allowing non-equilibrium fractionation at all $T < 0^{\circ}$ C, instead of only at $T < -20^{\circ}$ C, brings the simulated δD and deuterium excess values much further away from observations: if the condensate was mainly liquid between $T = -20^{\circ} \text{C}$ and $T = 0^{\circ} \text{C}$, this threshold would only have a minor impact.

With the implementation of a new ice nucleation scheme (Shi, Liu, & Zhang, 2015; Wang, Liu, Hoose, & Wang, 2014), as well as a new microphysics scheme (Gettelman, 2015), the ice bias has been greatly improved in newer versions of CAM (Bogenschutz et al., 2018). We therefore expect a better agreement between the modeled and observed δD and deuterium excess without the need for reducing naai, epsi, or deactivating non-equilibrium fractionation at T > -20°C in the isotope-enabled version of CAM6 that is currently under development.

4.2 Neglected processes

500

501

502

503

504

505

507

510

511

512

513

514

515

516

517

518

519

520

521

522

523

524

525

527

530

531

One process that has been neglected in the discussion so far is evaporation from the ocean or land. Since evaporation is the only process involving strong non-equilibrium fractionation apart from ice and mixed-phase cloud formation, the deuterium excess is commonly used as a proxy for moisture source conditions (e.g., Jouzel, Merlivat, & Lorius, 1982; Uemura et al., 2012; Vimeux, Masson, Jouzel, Stievenard, & Petit, 1999). From

532

533

534

535

536

537

538

539

542

543

544

545

546

547

548

551

552

553

554

555

556

557

558

561

562

a Rayleigh perspective, moisture source conditions determine the initial isotopic composition of the air parcel, while meteorological conditions during cloud formation determine how the isotopic composition of the air parcel evolves. For Antarctic precipitation, moisture mainly originates from the ocean (Sodemann & Stohl, 2009). Previous studies have shown that the wind speed dependent formulation by Merlivat and Jouzel (1979) that is used in iCAM5 for evaporation from the ocean does not represent non-equilibrium fractionation correctly (Bonne et al., 2019; Pfahl & Wernli, 2009; Uemura, Barkan, Abe, & Luz, 2010). This is why in this study we focus on the slope between δD and deuterium excess and not on the absolute values. However, the isotopic composition of the initial vapor can also influence the slope, due to the nonlinearity of the δ -scale (Dütsch et al., 2017; Markle et al., 2017). We test this with the Rayleigh equations (1 and 2) by adding -10% and +10% to the initial δD of the air parcels, corresponding to an initial deuterium excess of -10% and +10%, respectively. As Figure 10 shows, a higher initial deuterium excess in vapor unsurprisingly leads to a higher deuterium excess in the condensate, but the slope between δD and deuterium excess is nearly independent of the initial values. We therefore expect very similar results with regards to the slope between δD and deuterium excess for different formulations of fractionation during evaporation from the ocean or land.

By using the isotope ratios of precipitation from iCAM5, we also neglect potential postdepositional processes. Recent studies from Greenland and Antarctica show that isotopic exchanges between snow and water vapor (Steen-Larsen et al., 2014), fractionation during sublimation (Madsen et al., 2019; Ritter et al., 2016), and snow metamorphism (Casado et al., 2018) may alter the isotope ratios in surface snow, especially at low accumulation sites. Due to the snow depth limit of $H_{max} = 1$ m snow water equivalent in our version of CLM4 (see Section 2.1), the simulated snow pack mainly reflects the initial isotopic composition instead of the signal from precipitation, and it is not possible to meaningfully account for postdepositional processes. In a revised version of CLM4 (van Kampenhout et al., 2017), the snow pack is allowed to refresh from the top, and any excess mass is removed from the lowest snow layer instead. Including this new treatment of snow in the isotope version of CLM4 (iCLM4) (Wong et al., 2017) will be the focus of future work.

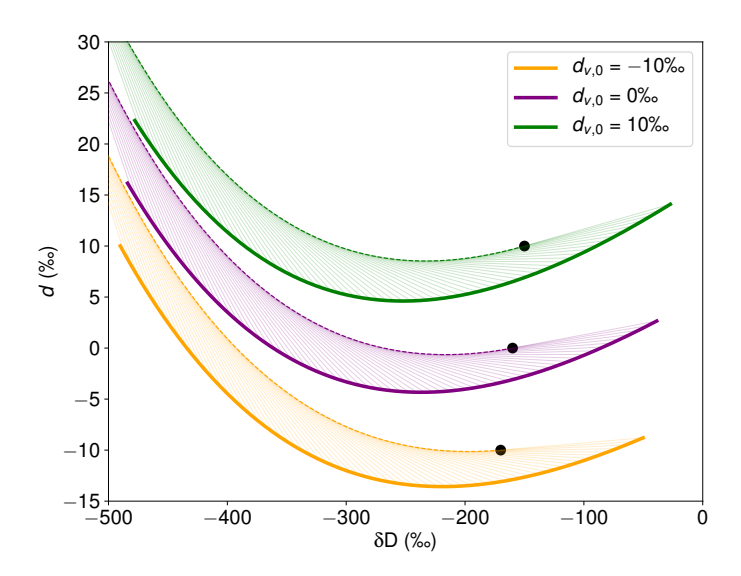


Figure 10. Evolution of δD and deuterium excess in water vapor (dashed lines) and condensate (solid lines) during Rayleigh condensation for different initial deuterium excess values $(d_{v,0})$ and $Si = 1 - 0.004 \cdot T$. The black dots depict the initial isotopic composition of the water vapor and the thin lines connect the isotopic composition of the condensate with the isotopic composition of the vapor it originates from.

5 Conclusions

The isotope version of the Community Atmosphere Model version 5 (iCAM5) is one of a few isotope-enabled Atmospheric General Circulation Models whose microphysics scheme does not apply saturation adjustment for the ice phase and therefore allows supersaturation with respect to ice. In this study we adapted iCAM5 to compute non-equilibrium fractionation during ice and mixed-phase cloud formation based on the supersaturation predicted by the microphysics scheme (the real supersaturation, Si_{real}) instead of the commonly-applied parameterization of supersaturation with respect to ice as a linear function of temperature (the parameterized supersaturation, Si_{param}).

A comparison between simulations using the real supersaturation and simulations using the parameterized supersaturation showed that a linear function oversimplifies the dependence of supersaturation with respect to ice on temperature, and that differences between the real and the parameterized supersaturation are reflected in deuterium excess in Antarctic precipitation. The average relation between δD and deuterium excess was nevertheless well reproduced by the simulations using the parameterized supersaturation, when properly tuned. Thus, a linear function of temperature tuned to match

isotope measurements may be a reasonable approximation of supersaturation with respect to ice. However, for a more physically realistic treatment of non-equilibrium fractionation and to adequately represent microphysical changes that are independent of temperature, using the real supersaturation is preferable.

Our results also showed that with the real supersaturation stable water isotopes can constrain microphysical parameters that influence supersaturation with respect to ice in the model. Reducing the number of active aerosols for ice nucleation (naai) or the Wegener-Bergeron-Findeisen time scale for the growth of ice crystals (epsi) improved the relation between δD and deuterium excess compared to observations, which is in agreement with previous findings showing that CAM5 overestimates the fraction of ice in mixed-phase clouds.

In summary, while the parameterization of supersaturation with respect to ice as a linear function of temperature may lead to reasonable results with the right tuning, using the real supersaturation to compute non-equilibrium fractionation ties the isotopes more closely to the model microphysics, which on the one hand facilitates interpretations of isotope measurements in paleoarchives, and on the other hand makes isotopes more useful observational constraints.

Acknowledgments

This work was funded by the Swiss National Science Foundation (SNSF; project number P2EZP2_178439). We would like to acknowledge high-performance computing support from Cheyenne (doi:10.5065/D6RX99HX) provided by NCAR's Computational and Information Systems Laboratory, sponsored by the National Science Foundation. Furthermore we thank Hugh Morrison, Andrew Gettelman, Blaž Gasparini and Bradley R. Markle for helpful discussions on microphysics and isotopes, and two anonymous reviewers for their constructive comments, which helped to improve the manuscript. iCESM is publicly accessible at https://github.com/NCAR/iCESM1.2. Model output data and scripts to create the figures are available at https://doi.org/10.5281/zenodo.3374014.

References

Blossey, P. N., Kuang, Z., & Romps, D. M. (2010). Isotopic composition of water in the tropical tropopause layer in cloud-resolving simulations of an idealized tropical circulation. *J. Geophys. Res.*, 115, D24309. doi:

```
10.1029/2010JD014554
```

- Bogenschutz, P. A., Gettelman, A., Hannay, C., Larson, V. E., Neale, R. B.,
- Craig, C., & Chen, C.-C. (2018). The path to CAM6: coupled simula-
- tions with CAM5.4 and CAM5.5. Geosci. Model Dev., 11, 235–255. doi:
- 10.5194/gmd-11-235-2018
- Bonne, J.-L., Behrens, M., Meyer, H., Kipfstuhl, S., Rabe, B., Schönicke, L., ...
- Werner, M. (2019). Resolving the controls of water vapour isotopes in the
- Atlantic sector. Nat. Commun., 10, 1632. doi: 10.1038/s41467-019-09242-6
- Brady, E., Stevenson, S., Bailey, D., Liu, Z., Noone, D., Nusbaumer, J., ... Zhu, J.
- 619 (2019). The connected isotopic water cycle in the Community Earth System
- 620 Model version 1. J. Adv. Model. Earth Sy.. doi: 10.1029/2019MS001663
- Bretherton, C. S., & Park, S. (2009). A new moist turbulence parameterization in
- the Community Atmosphere Model. J. Climate, 22(12), 3422–3448. doi: 10
- .1175/2008JCLI2556.1
- Buiron, D., Stenni, B., Chappellaz, J., Landais, A., Baumgartner, M., Bonazza,
- M., ... Udisti, R. (2012). Regional imprints of millennial variability dur-
- ing the MIS 3 period around Antarctica. Quat. Sci. Rev., 48, 99–112. doi:
- 627 10.1016/j.quascirev.2012.05.023
- Buizert, C., Sigl, M., Severi, M., Markle, B. R., Wettstein, J. J., McConnell, J. R.,
- 529 ... Steig, E. J. (2018). Abrupt ice-age shifts in southern westerly winds
- and Antarctic climate forced from the north. Nature, 563 (7733), 681. doi:
- 631 10.1038/s41586-018-0727-5
- 632 Casado, M., Landais, A., Picard, G., Münch, T., Laepple, T., Stenni, B., ... Jouzel,
- J. (2018). Archival processes of the water stable isotope signal in East Antarc-
- tic ice cores. Cryosphere, 12(5), 1745–1766. doi: 10.5194/tc-12-1745-2018
- 655 Cesana, G., Waliser, D. E., Jiang, X., & Li, J.-L. F. (2015). Multimodel evaluation
- of cloud phase transition using satellite and reanalysis data. J. Geophys. Res.
- 637 Atmos., 120(15), 7871–7892. doi: 10.1002/2014JD022932
- ⁶³⁸ Craig, H., & Gordon, L. I. (1965). Deuterium and oxygen 18 variations in the ocean
- and the marine atmosphere. In Stable isotopes in oceanographic studies and
- paleo-temperatures (pp. 9–130). Pisa, Italy: Lab. Geol. Nucl.
- Dansgaard, W. (1964). Stable isotopes in precipitation. Tellus, 16, 436–468. doi: 10
- .3402/tellusa.v16i4.8993

- Dansgaard, W., Johnsen, S. J., Clausen, H. B., Dahl-Jensen, D., Gundestrup, N. S.,
- Hammer, C. U., ... Bond, G. (1993). Evidence for general instability of
- past climate from a 250-kyr ice-core record. Nature, 364, 218–220. doi:
- 10.1038/364218a0
- DeMott, P. J., Prenni, A. J., Liu, X., Kreidenweis, S. M., Petters, M. D., Twohy,
- 648 C. H., ... Rogers, D. C. (2010). Predicting global atmospheric ice nuclei
- distributions and their impacts on climate. Proc. Natl. Acad. Sci., 107(25),
- 650 11217–11222. doi: 10.1073/pnas.0910818107
- Dütsch, M., Pfahl, S., & Sodemann, H. (2017). The impact of nonequilibrium and
- equilibrium fractionation on two different deuterium excess definitions. J. Geo-
- phys. Res. Atmos., 122, 12732–12746. doi: 10.1002/2017JD027085
- Eckstein, J., Ruhnke, R., Pfahl, S., Christner, E., Diekmann, C., Dyroff, C., ...
- Braesicke, P. (2018). From climatological to small-scale applications: simulat-
- ing water isotopologues with ICON-ART-Iso (version 2.3). Geosci. Model Dev.,
- 657 11, 5113-5133. doi: 10.5194/gmd-11-5113-2018
- EPICA Community Members. (2006). One-to-one coupling of glacial climate vari-
- ability in Greenland and Antarctica. Nature, 444 (7116), 195–198. doi: 10
- .1038/nature05301
- Field, R. D., Kim, D., LeGrande, A. N., Worden, J., Kelley, M., & Schmidt, G. A.
- 662 (2014). Evaluating climate model performance in the tropics with retrievals
- of water isotopic composition from Aura TES. Geophys. Res. Lett., 41, 6030-
- 6036. doi: 10.1002/2014GL060572
- Genthon, C., Piard, L., Vignon, E., Madeleine, J.-B., Casado, M., & Gallée, H.
- 666 (2017). Atmospheric moisture supersaturation in the near-surface atmosphere
- at Dome C, Antarctic Plateau. Atmos. Chem. Phys., 17(1), 691–704. doi
- 10.5194/acp-17-691-2017
- 669 Gettelman, A. (2015). Putting the clouds back in aerosol-cloud interactions. Atmos.
- 670 Chem. Phys., 15(21), 12397–12411. doi: 10.5194/acp-15-12397-2015
- Gettelman, A., Liu, X., Ghan, S. J., Morrison, H., Park, S., Conley, A. J., . . . Li, J.-
- L. F. (2010). Global simulations of ice nucleation and ice supersaturation with
- an improved cloud scheme in the Community Atmosphere Model. J. Geophys.
- Res. Atmos., 115, D18216. doi: 10.1029/2009JD013797
- Hoffmann, G., Werner, M., & Heimann, M. (1998). Water isotope module of

```
the ECHAM atmospheric general circulation model: A study on timescales
676
            from days to several years.
                                              J. Geophys. Res., 103, 16871–16896.
                                                                                         doi:
677
            10.1029/98JD00423
678
       Horita, J., & Wesolowski, D. J.
                                           (1994).
                                                        Liquid-vapor fractionation of oxygen
679
            and hydrogen isotopes of water from the freezing to the critical temper-
680
                         Geochim. Cosmochim. Acta, 58(16), 3425–3437.
                                                                                doi: 10.1016/
            ature.
681
            0016-7037(94)90096-5
      Hurrell, J. W., Hack, J. J., Shea, D., Caron, J. M., & Rosinski, J. (2008). A new sea
683
            surface temperature and sea ice boundary dataset for the Community Atmo-
            sphere Model. J. Climate, 21 (19), 5145-5153. doi: 10.1175/2008JCLI2292.1
       Hurrell, J. W., Holland, M. M., Gent, P. R., Ghan, S., Kay, J. E., Kushner, P. J.,
686
            ... Marshall, S.
                                (2013).
                                          The community earth system model: a framework
687
            for collaborative research.
                                          Bull. Am. Meteorol. Soc., 94(9), 1339–1360.
688
            10.1175/BAMS-D-12-00121.1
689
       Joussaume, S., Jouzel, J., & Sadourny, R.
                                                    (1984).
                                                              A general circulation model of
690
            water isotope cycles in the atmosphere.
                                                        Nature, 311, 24–29.
                                                                                doi: 10.1038/
691
            311024a0
692
       Jouzel, J., Masson-Delmotte, V., Cattani, O., Dreyfus, G., Falourd, S., Hoffmann,
            G., ... Wolff, E. W.
                                    (2007).
                                               Orbital and millennial Antarctic climate vari-
            ability over the past 800,000 years.
                                                      Science, 317(5839), 793-796.
                                                                                         doi:
            10.1126/science.1141038
696
       Jouzel, J., & Merlivat, L. (1984). Deuterium and oxygen 18 in precipitation: Mod-
697
            eling of the isotopic effects during snow formation.
                                                                   J. Geophys. Res., 89(D7),
698
            11749–11757. doi: 10.1029/JD089iD07p11749
699
       Jouzel, J., Merlivat, L., & Lorius, C. (1982). Deuterium excess in an East Antarctic
700
            ice core suggests higher relative humidity at the oceanic surface during the last
701
            glacial maximum. Nature, 299, 688–691. doi: 10.1038/299688a0
702
      Kahle, E. C., Holme, C., Jones, T. R., Gkinis, V., & Steig, E. J.
                                                                           (2018).
                                                                                      A gen-
703
            eralized approach to estimating diffusion length of stable water isotopes
                                     J. Geophys. Res. Earth Surf., 123, 2377–2391.
            from ice-core data.
                                                                                         doi:
```

(2016). Evaluating and improving cloud phase in the Community

Kay, J. E., Bourdages, L., Miller, N. B., Morrison, A., Yettella, V., Chepfer, H., &

10.1029/2018JF004764

706

707

708

```
Atmosphere Model version 5 using spaceborne lidar observations. J. Geophys.
709
            Res. Atmos., 121(8), 4162–4176. doi: 10.1002/2015JD024699
710
       Komurcu, M., Storelvmo, T., Tan, I., Lohmann, U., Yun, Y., Penner, J. E., ...
711
            Takemura, T.
                               (2014).
                                           Intercomparison of the cloud water phase among
712
                                       J. Geophys. Res. Atmos., 119(6), 3372-3400.
            global climate models.
                                                                                        doi:
713
            10.1002/2013JD021119
714
      Lamarque, J.-F., Bond, T. C., Eyring, V., Granier, C., Heil, A., Klimont, Z., ...
715
            van Vuuren, D. P.
                                   (2010).
                                              Historical (1850–2000) gridded anthropogenic
716
            and biomass burning emissions of reactive gases and aerosols: method-
            ology and application.
                                         Atmos. Chem. Phys, 10(15), 7017-7039.
                                                                                        doi:
718
            10.5194/acp-10-7017-2010
719
      Lamarque, J.-F., Kyle, G. P., Meinshausen, M., Riahi, K., Smith, S. J., van Vu-
720
            uren, D. P., ... Vitt, F.
                                      (2011). Global and regional evolution of short-lived
721
            radiatively-active gases and aerosols in the Representative Concentration Path-
722
            ways. Clim. Change, 109, 191–212. doi: 10.1007/s10584-011-0155-0
723
      Landais, A., Masson-Delmotte, V., Stenni, B., Selmo, E., Roche, D. M., Jouzel, J.,
724
            ... Popp, T. (2015). A review of the bipolar see–saw from synchronized and
725
            high resolution ice core water stable isotope records from Greenland and East
            Antarctica. Quat. Sci. Rev., 114, 18–32. doi: 10.1016/j.quascirev.2015.01.031
727
      Lee, J.-E., Fung, I., DePaolo, D. J., & Henning, C. C. (2007). Analysis of the global
728
            distribution of water isotopes using the NCAR atmospheric general circulation
729
            model. J. Geophys. Res., 112, D16306. doi: 10.1029/2006JD007657
730
      Liu, X., & Penner, J. E. (2005). Ice nucleation parameterization for global models.
731
            Meteorol. Z., 14(4), 499–514. doi: 10.1127/0941-2948/2005/0059
732
      Liu, X., Penner, J. E., Ghan, S. J., & Wang, M. (2007). Inclusion of ice microphysics
733
            in the NCAR Community Atmospheric Model version 3 (CAM3).
734
            20(18), 4526-4547. doi: 10.1175/JCLI4264.1
735
      Madsen, M. V., Steen-Larsen, H. C., Hörhold, M., Box, J., Berben, S., Capron, E.,
736
            ... Dahl-Jensen, D.
                                    (2019).
                                               Evidence of isotopic fractionation during va-
            por exchange between the atmosphere and the snow surface in Greenland.
                                                                                          J.
            Geophys. Res. Atmos.. (in press) doi: 10.1029/2018JD029619
739
       Majoube, M.
                        (1971).
                                   Fractionnement en oxygène 18 entre la glace et la vapeur
740
```

d'eau. J. Chim. Phys., 68, 625–636. doi: 10.1051/jcp/1971680625

741

- Markle, B. R., Steig, E. J., Buizert, C., Schoenemann, S. W., Bitz, C. M., Fudge,
- T. J., ... Sowers, T. (2017). Global atmospheric teleconnections during
- Dansgaard-Oeschger events. *Nat. Geosci.*, 10, 36–40. doi: 10.1038/ngeo2848
- Masson-Delmotte, V., Hou, S., Ekaykin, A., Jouzel, J., Aristarain, A., Bernardo,
- R. T., ... White, J. W. C. (2008). A review of Antarctic surface snow isotopic
- composition: observations, atmospheric circulation, and isotopic modeling. J.
- 748 Climate, 21(13), 3359–3387. doi: 10.1175/2007JCLI2139.1
- Mathieu, R., Pollard, D., Cole, J. E., White, J. W. C., Webb, R. S., & Thompson,
- S. L. (2002). Simulation of stable water isotope variations by the GENESIS
- GCM for modern conditions. J. Geophys. Res. Atmos., 107(D4), 4037. doi:
- 752 10.1029/2001JD900255
- Merlivat, L. (1978). Molecular diffusivities of $H_2^{16}O$, $HD^{16}O$, and $H_2^{18}O$ in gases. J.
- 754 Chem. Phys., 69, 2864–2871. doi: 10.1063/1.436884
- Merlivat, L., & Jouzel, J. (1979). Global climatic interpretation of the deuterium-
- oxygen 18 relationship for precipitation. J. Geophys. Res., 84 (C8), 5029–5033.
- doi: 10.1029/JC084iC08p05029
- Merlivat, L., & Nief, G. (1967). Fractionnement isotopique lors des changements
- d'état solide-vapeur et liquide-vapeur de l'eau à des températures inférieures à
- 760 0°C. Tellus, 19, 122–127. doi: 10.1111/j.2153-3490.1967.tb01465.x
- Meyers, M. P., DeMott, P. J., & Cotton, W. R. (1992). New primary ice-nucleation
- parameterizations in an explicit cloud model. J. Appl. Meteorol., 31(7), 708–
- 763 721. doi: $10.1175/1520-0450(1992)031\langle 0708:NPINPI\rangle 2.0.CO; 2$
- Morrison, H., & Gettelman, A. (2008). A new two-moment bulk stratiform cloud
- microphysics scheme in the Community Atmosphere Model, version 3 (CAM3).
- Part I: Description and numerical tests. J. Climate, 21(15), 3642–3659. doi:
- 767 10.1175/2008JCLI2105.1
- 768 Moyer, E. J., Irion, F. W., Yung, Y. L., & Gunson, M. R. (1996). ATMOS strato-
- spheric deuterated water and implications for troposphere-stratosphere trans-
- port. Geophys. Res. Lett., 23(17), 2385–2388. doi: 10.1029/96GL01489
- Neale, R. B., Chen, C.-C., Gettelman, A., Lauritzen, P. H., Park, S., Williamson,
- D. L., ... Taylor, M. A. (2010). Description of the NCAR community atmo-
- sphere model (CAM 5.0). NCAR Technical Note NCAR/TN-486+ STR, Natl.
- 774 Cent. for Atmos. Res., Boulder, CO, USA.

- Nusbaumer, J., Wong, T. E., Bardeen, C., & Noone, D. (2017). Evaluating hydrological processes in the Community Atmosphere Model Version 5 (CAM5) using stable isotope ratios of water. J. Adv. Model. Earth Sy., 9(2), 949–977. doi: 10.1002/2016MS000839
- Park, S., & Bretherton, C. S. (2009). The University of Washington shallow convection and moist turbulence schemes and their impact on climate simulations with the Community Atmosphere Model. *J. Climate*, 22(12), 3449–3469. doi: 10.1175/2008JCLI2557.1
- Park, S., Bretherton, C. S., & Rasch, P. J. (2014). Integrating cloud processes in the

 Community Atmosphere Model, version 5. *J. Climate*, 27(18), 6821–6856. doi:

 10.1175/JCLI-D-14-00087.1
- Petit, J. R., White, J. W. C., Young, N. W., Jouzel, J., & Korotkevich, Y. S. (1991).

 Deuterium excess in recent Antarctic snow. J. Geophys. Res., 96(D3), 5113–5122. doi: 10.1029/90JD02232
- Pfahl, S., & Wernli, H. (2009). Lagrangian simulations of stable isotopes in water vapor: An evaluation of nonequilibrium fractionation in the Craig-Gordon model. J. Geophys. Res., 114 (D20), D20108. doi: 10.1029/2009JD012054
- Prenni, A. J., Harrington, J. Y., Tjernström, M., DeMott, P. J., Avramov, A.,

 Long, C. N., ... Verlinde, J. (2007). Can ice-nucleating aerosols affect

 arctic seasonal climate? Bull. Amer. Meteor. Soc., 88(4), 541–550. doi:

 10.1175/BAMS-88-4-541
- Risi, C., Bony, S., Vimeux, F., & Jouzel, J. (2010). Water-stable isotopes in the LMDZ4 general circulation model: Model evaluation for present-day and past climates and applications to climatic interpretations of tropical isotopic records. J. Geophys. Res., 115, D12118. doi: 10.1029/2009JD013255
- Risi, C., Noone, D., Worden, J., Frankenberg, C., Stiller, G., Kiefer, M., . . . Sturm,

 C. (2012). Process-evaluation of tropospheric humidity simulated by general circulation models using water vapor isotopic observations: 2. Using
 isotopic diagnostics to understand the mid and upper tropospheric moist
 bias in the tropics and subtropics. J. Geophys. Res., 117, D05304. doi:
 10.1029/2011JD016623
- Ritter, F., Steen-Larsen, H. C., Werner, M., Masson-Delmotte, V., Orsi, A., Behrens,
 M., . . . Kipfstuhl, S. (2016). Isotopic exchange on the diurnal scale between

- near-surface snow and lower atmospheric water vapor at Kohnen station, East
 Antarctica. Cryosphere, 10, 1647–1663. doi: 10.5194/tc-10-1647-2016
- Rogers, R. R. (1979). A Short Course in Cloud Physics (Vol. 96). New York, NY,
 USA: Pergamon Press.
- Sagoo, N., & Storelymo, T. (2017). Testing the sensitivity of past climates to the indirect effects of dust. *Geophys. Res. Lett.*, 44 (11), 5807–5817. doi: 10.1002/
- Schmidt, G. A., Hoffmann, G., Shindell, D. T., & Hu, Y. (2005). Modeling atmospheric stable water isotopes and the potential for constraining cloud processes and stratosphere-troposphere water exchange. *J. Geophys. Res.*, 110 (D21314). doi: 10.1029/2005JD005790
- Schoenemann, S. W., Steig, E. J., Ding, Q., Markle, B. R., & Schauer, A. J. (2014).

 Triple water-isotopologue record from WAIS Divide, Antarctica: Controls on
 glacial-interglacial changes in ¹⁷O_{excess} of precipitation. *J. Geophys. Res.*,

 119(14), 8741–8763. doi: 10.1002/2014JD021770
- Shi, X., Liu, X., & Zhang, K. (2015). Effects of pre-existing ice crystals on cirrus clouds and comparison between different ice nucleation parameterizations with the Community Atmosphere Model (CAM5). Atmos. Chem. Phys., 15(3), 1503–1520. doi: 10.5194/acp-15-1503-2015
- Sime, L. C., Wolff, E. W., Oliver, K. I. C., & Tindall, J. C. (2009). Evidence for warmer interglacials in East Antarctic ice cores. *Nature*, 462(7271), 342. doi: 10.1038/nature08564
- Sodemann, H., & Stohl, A. (2009). Asymmetries in the moisture origin of Antarctic precipitation. *Geophys. Res. Lett.*, 36, L22803. doi: 10.1029/2009GL040242,
- Steen-Larsen, H. C., Masson-Delmotte, V., Hirabayashi, M., Winkler, R., Satow,

 K., Prié, F., ... Sveinbjörnsdottír, A. E. (2014). What controls the isotopic

 composition of Greenland surface snow? *Clim. Past*, 10(1), 377–392. doi:

 10.5194/cp-10-377-2014
- Stenni, B., Buiron, D., Frezzotti, M., Albani, S., Barbante, C., Bard, E., ... Udisti,

 R. (2011). Expression of the bipolar see-saw in Antarctic climate records

 during the last deglaciation. *Nat. Geosci.*, 4(1), 46. doi: 10.1038/ngeo1026
- Stenni, B., Masson-Delmotte, V., Selmo, E., Oerter, H., Meyer, H., Röthlisberger,
 R., ... Udisti, R. (2010). The deuterium excess records of EPICA Dome C

- and Dronning Maud Land ice cores (East Antarctica). Quat. Sci. Rev., 29(1),
 146–159. doi: 10.1016/j.quascirev.2009.10.009
- Tan, I., & Storelvmo, T. (2016). Sensitivity study on the influence of cloud microphysical parameters on mixed-phase cloud thermodynamic phase partitioning in CAM5. J. Atmos. Sci., 73(2), 709–728. doi: 10.1175/JAS-D-15-0152.1
- Tan, I., Storelymo, T., & Zelinka, M. D. (2016). Observational constraints on mixedphase clouds imply higher climate sensitivity. Science, 352(6282), 224–227.

 doi: 10.1126/science.aad5300
- Tindall, J. C., Valdes, P. J., & Sime, L. C. (2009). Stable water isotopes in HadCM3: Isotopic signature of El Niño-Southern Oscillation and the tropical amount effect. *J. Geophys. Res. Atmos.*, 114, D04111. doi: 10.1029/2008JD010825
- Uemura, R., Barkan, E., Abe, O., & Luz, B. (2010). Triple isotope composition of oxygen in atmospheric water vapor. *Geophys. Res. Lett.*, 37, L04402. doi: 10.1029/2009GL041960
- Uemura, R., Masson-Delmotte, V., Jouzel, J., Landais, A., Motoyama, H., & Stenni,
 B. (2012). Ranges of moisture-source temperature estimated from Antarctic
 ice cores stable isotope records over glacial-interglacial cycles. Clim. Past, 8,
 1109–1125. doi: 10.5194/cp-8-1109-2012
- van Kampenhout, L., Lenaerts, J. T. M., Lipscomb, W. H., Sacks, W. J., Lawrence,

 D. M., Slater, A. G., & van den Broeke, M. R. (2017). Improving the representation of polar snow and firn in the Community Earth System Model. *J. Adv.*Model. Earth Sy., 9(7), 2583–2600. doi: 10.1002/2017MS000988
- Vimeux, F., Masson, V., Jouzel, J., Stievenard, M., & Petit, J. R. (1999). Glacial—
 interglacial changes in ocean surface conditions in the Southern Hemisphere.

 Nature, 398, 410–413. doi: 10.1038/18860
- WAIS Divide Project Members. (2013). Onset of deglacial warming in West Antarctica driven by local orbital forcing. *Nature*, 500 (7463), 440–444. doi: 10.1038/
- WAIS Divide Project Members. (2015). Precise interpolar phasing of abrupt climate
 change during the last ice age. Nature, 520(7549), 661–665. doi: 10.1038/
 nature14401
- Wall, C. J., Hartmann, D. L., & Ma, P.-L. (2017). Instantaneous linkages be-

- tween clouds and large-scale meteorology over the Southern Ocean in observations and a climate model. *J. Climate*, 30(23), 9455–9474. doi:
- 876 10.1175/JCLI-D-17-0156.1
- Wang, Y., Liu, X., Hoose, C., & Wang, B. (2014). Different contact angle
- distributions for heterogeneous ice nucleation in the Community Atmo-
- spheric Model version 5. Atmos. Chem. Phys., 14 (19), 10411–10430. doi:
- 10.5194/acp-14-10411-2014
- Werner, M., Langebroek, P. M., Carlsen, T., Herold, M., & Lohmann, G. (2011).
- Stable water isotopes in the ECHAM5 general circulation model: Toward high-
- resolution isotope modeling on a global scale. J. Geophys. Res., 116, D15109.
- doi: 10.1029/2011JD015681
- Werner, M., Mikolajewicz, U., Heimann, M., & Hoffmann, G. (2000). Borehole
- versus isotope temperatures on Greenland: Seasonality does matter. Geophys.
- 887 Res. Lett., 27(5), 723–726. doi: 10.1029/1999GL006075
- Wong, T. E., Nusbaumer, J., & Noone, D. C. (2017). Evaluation of modeled
- land-atmosphere exchanges with a comprehensive water isotope fractiona-
- tion scheme in version 4 of the Community Land Model. J. Adv. Model. Earth
- Sy., 9(2), 978-1001. doi: 10.1002/2016MS000842
- Xie, S., Liu, X., Zhao, C., & Zhang, Y. (2013). Sensitivity of CAM5-simulated Arc-
- tic clouds and radiation to ice nucleation parameterization. J. Climate, 26(16),
- 5981–5999. doi: 10.1175/JCLI-D-12-00517.1
- Yoshimura, K., Kanamitsu, M., Noone, D., & Oki, T. (2008). Historical isotope sim-
- ulation using reanalysis atmospheric data. J. Geophys. Res., 113, D19108. doi:
- 10.1029/2008JD010074
- Young, K. C. (1974). The role of contact nucleation in ice phase initiation in
- 899 clouds. J. Atmos. Sci., 31(3), 768-776. doi: 10.1175/1520-0469(1974)031(0768:
- $TROCNI \ge 2.0.CO; 2$
- Zhang, G. J., & McFarlane, N. A. (1995). Sensitivity of climate simulations
- to the parameterization of cumulus convection in the Canadian Climate
- Centre general circulation model. Atmos. Ocean, 33(3), 407–446. doi:
- 10.1080/07055900.1995.9649539
- Zhu, J., Liu, Z., Brady, E., Otto-Bliesner, B., Zhang, J., Noone, D., ... Tabor,
- 906 C. (2017). Reduced ENSO variability at the LGM revealed by an isotope-

enabled Earth system model. Geophys. Res. Lett., 44(13), 6984–6992. doi: 10.1002/2017 GL 073406